Non-Intrusive Frequency Measurements with Laser Shadowgraphy and Event-Based Schlieren Imaging of Bluff-Body Wakes In Compressible Flow

M. Nüßle[1,*], F. Ebertz[2], N. Essig[1], C. Schulz[2], B. Weigand[1], C. Steinhausen[1]

1: Institute of Aerospace Thermodynamics, University of Stuttgart, Germany
2: Institute for Energy and Materials Processes, University of Duisburg-Essen, Germany
*Corresponding author: max.nuessle@itlr.uni-stuttgart.de

Keywords: Event-Based, Schlieren, Transonic Flow, Vortex Shedding.

ABSTRACT

Event-based imaging is an emerging technology in thermodynamics and fluid dynamics. In this work, we are leveraging an event-based camera with a conventional schlieren set-up to investigate the vortex shedding dynamics behind a blunt central injector in a transonic nozzle flow. We offer different methods to evaluate the data stream of the event-based camera. Standard Fourier methods are not directly applicable to this data due to a non-constant time step. Therefore, the data needs to be treated with special care. Clusters of on- and off-events alternate and show the periodic nature of the wake. Using a clustering algorithm on the event groups also provides an estimation of vortex shedding frequency. These results are compared with laser shadowgraphy, a second novel method to measure the vortex shedding frequency in the wake. Both approaches to measuring the vortex shedding frequency are agreeing with each other within $1\,\%$. They each offer a simple set-up with comparatively low cost for their high temporal resolution.

1. Introduction

Mixing processes in ramjet combustion chambers as well as in chemical flow reactors determine the efficiency and quality of the process. Therefore, the physical processes of mixing downstream of an injector in high Reynolds and Mach number flow is of great interest. Often the precursor or fuel is injected through a blunt injector centered in the flow channel. The mixing behavior and quality is dependent on the geometry of the injection and the flow conditions at the point of injection. Previous studies have compared different injector geometries and injection in the subsonic and supersonic region of a nozzle (Mohri et al., 2015; Wohler et al., 2014; Richter et al., 2019). The blunt trailing edge of the injector leads to an oscillating wake region shedding vortices periodically (Richter et al., 2017; Williamson, 1996). These highly unsteady processes are dominating the mixing in the wake of the injector. Therefore, knowing the vortex shedding frequency is of great

interest. In earlier works a laser schlieren setup as well as a high-speed shadowgraphy method was used to measure the shedding frequency optically (Richter et al., 2017). Measurements with high-speed cameras usually generate large amounts of data while requiring image processing to generate quantifiable data. For this study we use a simplified experimental setup derived from Richter et al. (2017). Furthermore, we introduce different techniques of frequency analysis based on schlieren photography with an event-based camera.

Interest in event-based cameras recently increased in fluid mechanics contexts (Shiba et al., 2023; Willert & Klinner, 2022; Willert, 2023). In contrast to classical frame-based cameras, event-based cameras do not record full arrays of pixel values at a set frequency. Up to a certain degree, every pixel in an event-based camera can generate on- and off-events at separate times. An on-event is generated when the change of intensity at a given pixel surpasses a certain threshold. An off-event is generated when the intensity drops by a certain level. This means that an event-based camera generates a stream of data containing the pixel coordinates, type of event and event time. The working principle of event-based cameras permits high time resolution and, compared to traditional sensors, low data rate (Gallego et al., 2022).

2. Experimental Conditions

The test section is comprised of a convergent-divergent Laval nozzle with a rectangular cross section. An gas injector is placed in the middle of the nozzle geometry. It injects a toluene-seeded nitrogen flow into the subsonic section of the nozzle flow. A schematic side view is depicted in Figure 1. The main flow through the nozzle is comprised of dry air at a total pressure of $p_t = 2.5\,\mathrm{bar}$ and a total temperature of $T_t = 380\,\mathrm{K}$. These leads to a maximum Mach number at the end of the nozzle section of $M = 1.7$. The test facility at the ITLR permits continuous airflow at operating conditions. The total injector mass flow was kept at a steady rate of $\dot{m}_{inj} = 0.75\,\frac{\mathrm{g}}{\mathrm{s}}$. Toluene vapor comprised $40\,\%$ while nitrogen comprised $60\,\%$ of the total injector mass flow. Toluene was vaporized in a BrooksDLI vaporizing module.

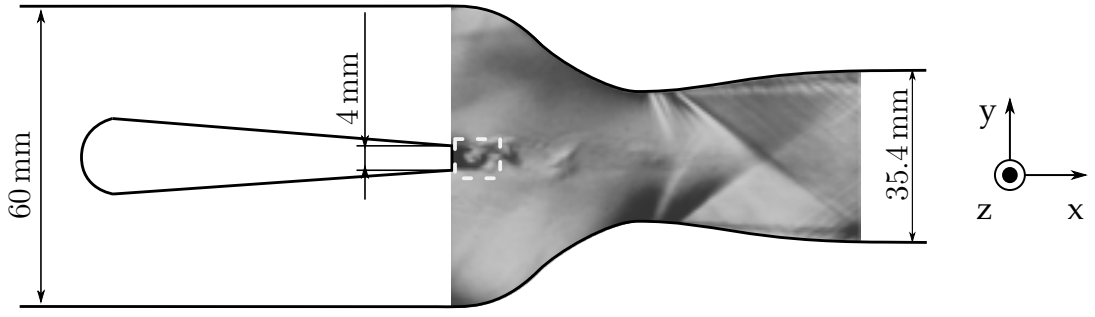

Figure 1. Schematic side view of the test section overlain with a short-time illuminated schlieren image adapted from (Richter et al., 2022). The marked region shows the region of interest for event-based schlieren.

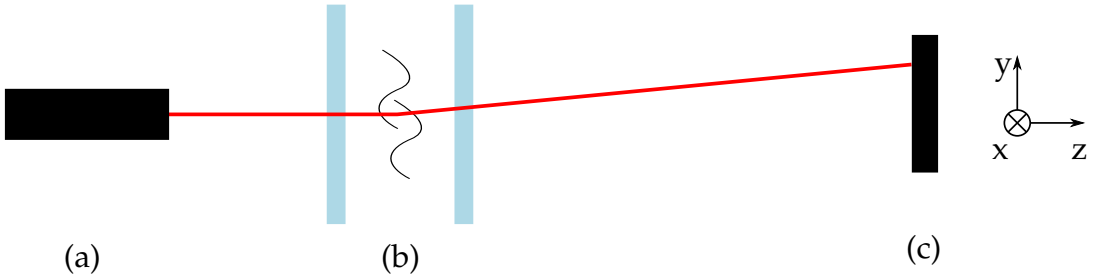

Figure 2. Schematic setup of laser shadowgraphy (a) collimated beam of a laser diode (b) schlieren object (c) segmented photodiode.

3. Laser Shadowgraphy

Traditional shadowgraphy requires collimation of an extended light source. As the laser beam is already collimated this is not necessary anymore. Hence, the setup simplifies to just a laser and the photodiode. A schematic of the setup is shown in Figure 2. In shadowgraphy, a second gradient in refractive index in the medium directly translates to a displacement on the detector (Settles, 2001). Therefore, the displacement of the laser beam on the detector can be used as an indicator of the vortex shedding. In contrast to classical shadowgraphy the method presented here only provides a point measurement.

The laser shadowgraphy setup is comprised of a Thorlabs PL202 collimated diode laser with a wavelength of $\lambda = 638\,\mathrm{nm}$ at an output power of $P = 0.93\,\mathrm{mW}$ and a Thorlabs PDQ80A segmented photodiode. The photodiode outputs a signal for x and y separately. The diode signals were recorded using a LeCroy WaveSurfer 104MXs-B oscilloscope at a sample rate of $f_s = 100\,\mathrm{kHz}$.

For analysis, only the x-component of the laser shadowgraphy signal is used. Due to the high noise within the signal it was analyzed using Welch's method, of computing a periodogram (Welch, 1967). With Welch's method the signal is analyzed utilizing the fast Fourier transform in multiple sections. Each section overlaps the previous one by half. The resulting periodograms are then averaged. Each section is 512 samples long and windowed using a Hann window as well as zero-padded to 2^{12} total samples to increase the frequency resolution. An exemplary section of the laser shadowgraphy signal is shown in Figure 3 (a) together with the corresponding periodogram in Figure 3 (b). In the periodogram it can be seen that the highest peak around $7\,\mathrm{kHz}$ is split into two sub-peaks. These are located at $6958\,\mathrm{Hz}$ as well as $7397\,\mathrm{Hz}$. At approximately multiples of $7\,\mathrm{kHz}$ up to at least $28\,\mathrm{kHz}$ further peaks can be seen. They are, however wider in frequency and shallower. In total the baseline of the periodogram shows a steady decline.

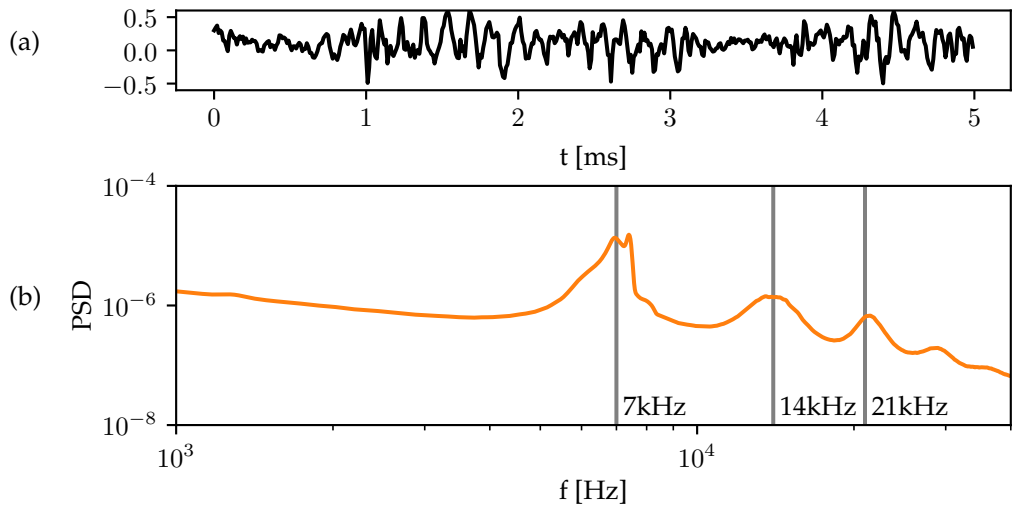

Figure 3. Frequency analysis of the laser schlieren data. (a) example section of the signal given by the photodiode (b) Welch periodogram computed from the full signal.

4. Event-Based Schlieren Imaging

For schlieren imaging, two achromatic lenses with a diameter of $100\,\mathrm{mm}$ are used. Both lenses have a focal length of $f_l = 1000\,\mathrm{mm}$. An LED-array behind a horizontal slit is used as a light source. The schlieren edge is realized with a horizontal slit. The image is then captured with the event-based camera (Prophesee EVK 4 HD). Overall, the measurement time in this case is $t = 0.1\,\mathrm{s}$. A schematic of the set-up is shown in Figure 4.

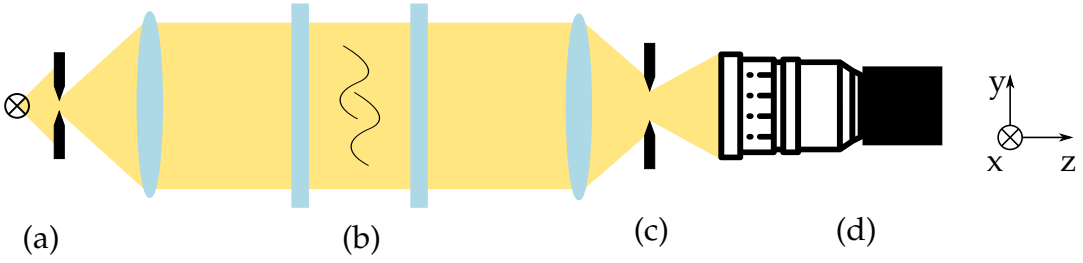

Figure 4. Schematic setup of event-based schlieren. (a) light source and slit (b) schlieren object (c) schlieren edge (d) event-based camera with lens.

For a time frame of $30\,\mu\mathrm{s}$ all events in the injector wake region are shown in Figure 5 (a). On-events are shown in blue while off-events are shown in red. Figure 5 shows symmetry between the on- and off-events in y-direction. As the event-based camera provides a time series of events they can also be analyzed with respect to their temporal distribution as shown in Figure 5 (b). It can be seen that on- and off-events form groups that appear in alternating, discrete time intervals.

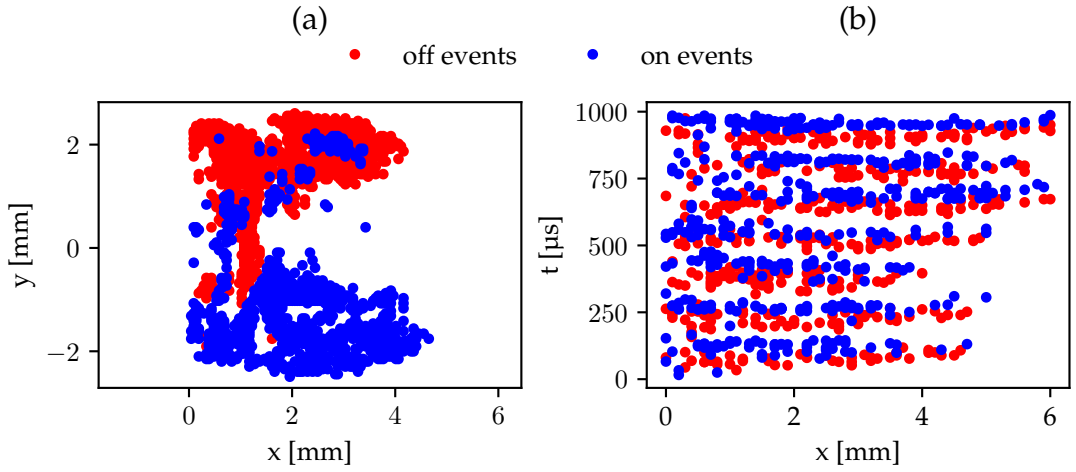

Figure 5. On- and off-events from event-based schlieren at the injector trailing edge in. (a) side view of the events in the $x-y$ plane within a time frame of $50\,\mu s$. Only every 20th event is shown (b) view of the events on the $x-t$ plane.

4.1. Frequency Analysis

The alternating occurrence of on- and off-events, as seen in Figure 5 (b), already shows the periodic oscillations of the injector wake. To be able to use frequency analysis techniques on the event stream as shown further processing steps are necessary. First, each on-event is assigned a weight of 1, while each off-event is assigned a weight of -1. Then the event data is summed vertically along the y-coordinate. This can also be understood as a weighted sum of all events in a specific row of the camera sensor for the whole measurement time. In Figure 6 (a) we show the regions for a sum of events smaller than 1 in red, larger than 1 in blue and in between in gray. As the clusters are at a constant time we further sum these results along the x-axis. This yields the weighted number of events that were registered at a certain time. This is shown in Figure 6 (b). The time signal obtained by this method can now be analyzed. However, special care must be taken in the frequency analysis of this signal as the time steps between two data points is not necessarily constant as the event-based cameras does not record on a fixed time interval. Consequently, 'classical' methods of frequency analysis like discrete Fourier transformation cannot be employed without special care as these algorithms require constant time steps. For frequency analysis of signals with non-uniform time steps the Lomb-Scargle periodogram can be used (Lomb, 1976; Scargle, 1982). For computation of the periodogram with the Lomb-Scargle method a frequency grid has to be specified. In this case we use a grid ranging from $0.1\,\mathrm{Hz}$ to $42\,\mathrm{kHz}$ with a spacing of $10\,\mathrm{Hz}$. The resulting spectrum is shown shown in Figure 7 (b). Although the noise floor is high, three peaks can be seen clearly, located around $7\,\mathrm{kHz}$ and its multiples. The first peak is split into two sub-peaks at $6940\,\mathrm{Hz}$ and $7440\,\mathrm{Hz}$.

As the vertical sum of events, as shown in Figure 5 (a), clearly shows a periodic nature it lends itself to analysis with two-dimensional Fast Fourier Transform (FFT). As described earlier this is only

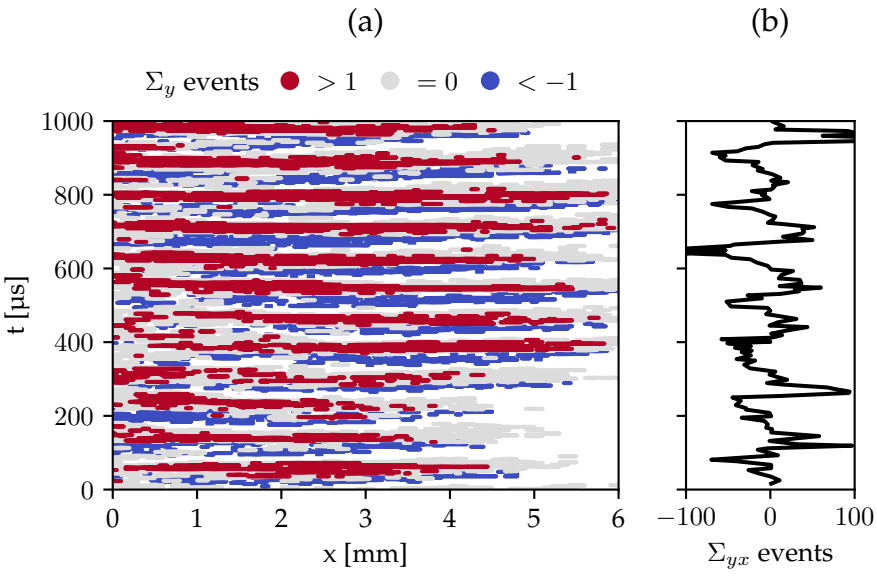

Figure 6. Weighted sum of events: every on-event is a 1, every off-event a -1 (a) vertical sum of on- and off-events along constant y (b) weighted vertical and axial sum of on- and off-events along x and y.

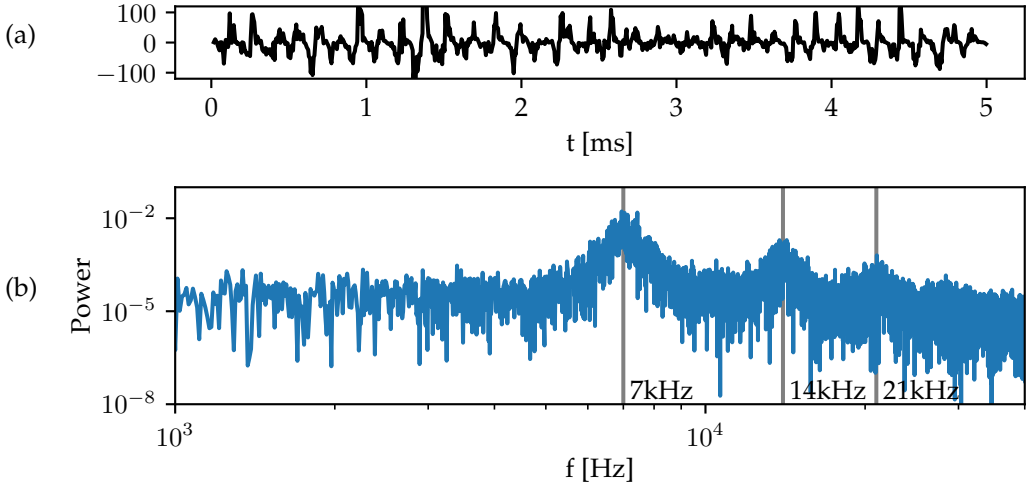

Figure 7. Frequency analysis of the axial and vertical sum of events. (a) Signal resulting from axial and vertical sum of events. (b) Lomb-Scargle periodogram computed from the sum. Clear peaks can be seen around 7 kHz and its higher harmonics.

allowed constant time step as well as a constant spacing. Therefore, the data was interpolated using nearest neighbor interpolation onto a regular grid. Afterwards the data was also zero-padded to 2^{12} data points in time as well as 2^8 data points in x and windowed with a Hann window. The resulting power distribution is shown in Figure 8 (b). The power distribution is almost symmetrical about the wave number $0\,\frac{1}{\mathrm{mm}}$. The power at wave number $0\,\frac{1}{\mathrm{mm}}$ is shown in Figure 8 (c). It shows a peak at $6957\,\mathrm{Hz}$ as well as two at its multiples.

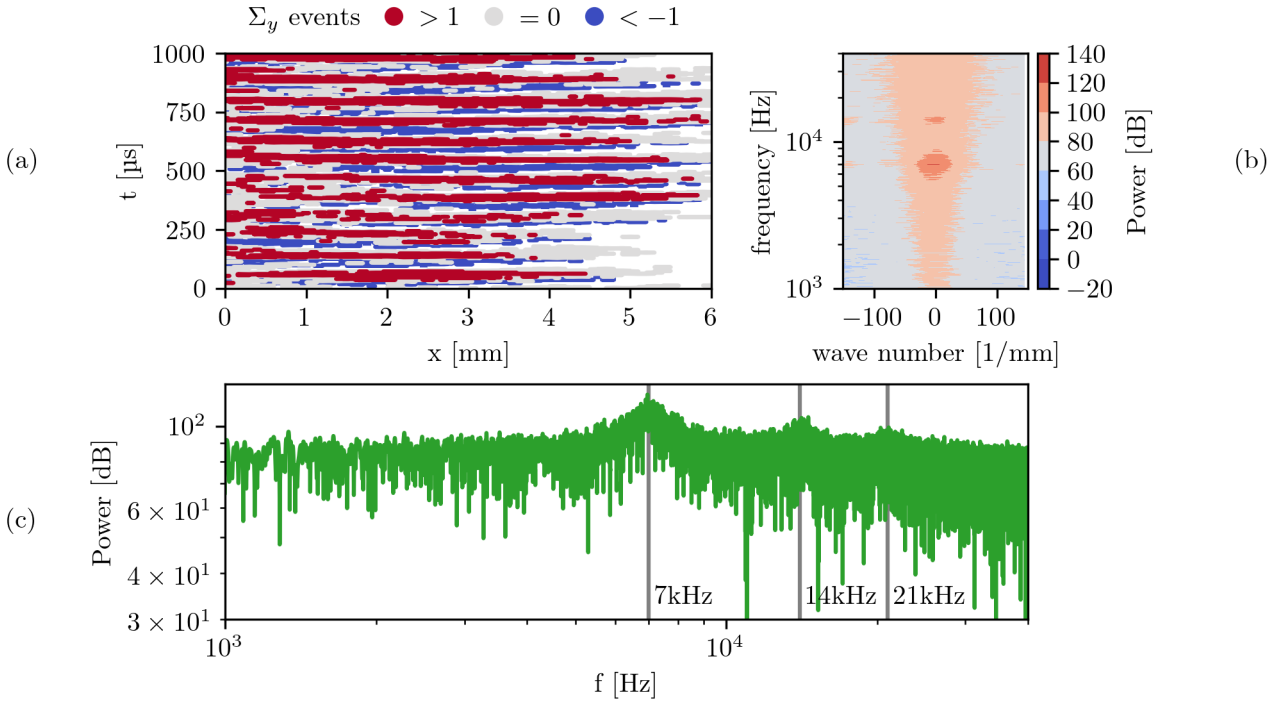

Figure 8. Frequency analysis of the event-based schlieren data. (a) vertival sum of events as shown in Figure 6 (b) 2D FFT of the sum of the events as shown in (a) power distribution of the 2D FFT at a wavenumber of $0\,\frac{1}{\mathrm{mm}}$

.

4.2. Automatic Clustering

Visually, the events form coherent clusters in the $x-t$ plane. The number of clusters in a known time frame, therefore, also corresponds to the shedding frequency. As the data contains a large amount of clusters, counting them manually is not feasible. In consequence, clustering algorithms need to be used to assign clusters to the data points. In this work, we used the clustering algorithm DBSCAN (Ester et al., 1996). DBSCAN can assign points to clusters even though the number of clusters is not known in advance. It marks data points either as a core point of a cluster, a non-core point of a cluster or as noise. For this to work, efficiently the parameters to the algorithm were manually tuned on a small subset of the data that we were able to visually inspect. For

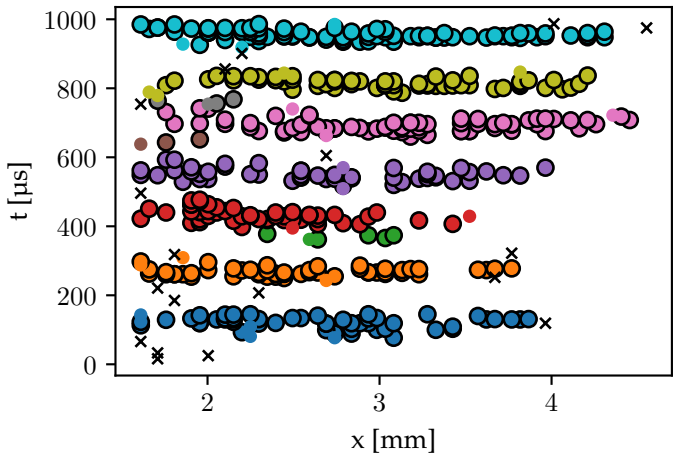

Figure 9. Clusters obtained with DBSCAN denoted by different colors. Points marked with and 'x' are considered noise by DBSCAN. Every 20th event is shown.

determination of the frequency, only on-events were handed to the clustering algorithm. Results from clustering are shown on a subset o the data in Figure 9. For further processing small clusters were discarded as well as points categorized as noise. With these settings the, algorithm finds 714 clusters of on-events in the full measurement time of 0.1 s which corresponds to a frequency of 7140 Hz.

5. Conclusion and Discussion

Comparing the different methods shows a very good agreement between the histograms as can be seen in Figure 10. All three displayed methods show the same dominant frequency besides a very small deviation. They also all show harmonics of this frequency. Also the frequency obtained by clustering methods agrees very well with the other methods. A comparison of the measured frequencies as well as their relative error is shown in Table 1.

Table 1. Vortex shedding frequencies obtained by different measurement methods.

	laser shadowgraphy	events 1D	2d FFT events	clustering
f first peak	6958 Hz	6940 Hz	6957 Hz	7140 Hz
relative error	reference	−0.25 %	−0.01 %	2.62 %

Notable is that with laser shadowgraphy as well as with the time series of weighted event sum a split is observed in the first frequency peak. This has not been observed in earlier measurements at the ITLR. This is especially notable because the corresponding measurements have been conducted on different days. This makes it seem like the splitting of the peak is a characteristic of this

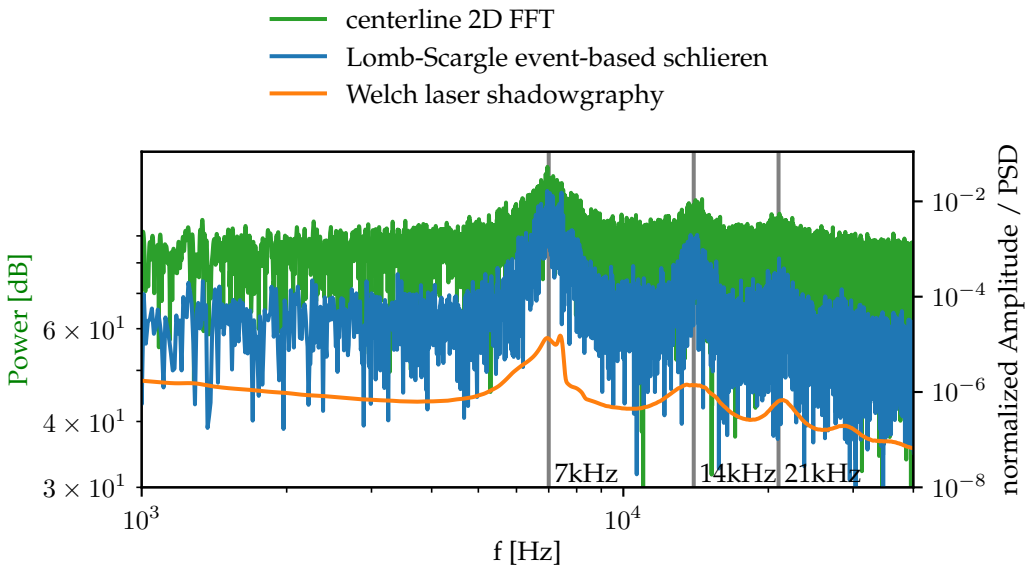

Figure 10. Comparison between the frequency analysis of the event-based schlieren data with the laser shadowgraphy data.

experiment.

While established methods of frequency analysis can be used with laser shadowgraphy some processing steps are necessary for analyzing event-based data in the same way. Here, we achieved this by computing weighted sums of events. Still, common methods like Fourier analysis need a fixed time step between measurements. However, interpolating data can lead to parasitic frequencies in the frequency spectrum.

It could be shown that laser shadowgraphy and event-based schlieren methods provide a good option for investigating transient fluid flow phenomena. With both methods, a very high temporal resolution can be achieved while also being significantly cheaper than a high-speed camera at similar frame rates would be. Additionally, both presented methods produce less data compared to a high-speed camera within the same measurement time. In contrast to laser shadowgraphy event-based schlieren additionally provides the possibility to generate pseudo-images to visualize the captured structures.

Categorizing events into contiguous clusters with clustering algorithms might offer an interesting approach for tracking structures in flows in general.

Acknowledgments

The authors like to acknowledge funding by the German Research Foundation with the project number 250957080.

Nomenclature

f	Frequency [Hz]
f_l	Focal length [m]
M	Mach number [-]
$\dot{m}$	Mass flow [$\frac{\mathrm{kg}}{\mathrm{s}}$]
P	Power [W]
PSD	Power spectral density [-]
p_t	Total pressure [Pa]
T_t	Total temperature [K]
t	Time [s]
x, y	Coordinates [m]
λ	Wave length [m]

References

Ester, M., Kriegel, H.-P., Sander, J., & Xu, X. (1996). A density-based algorithm for discovering clusters in large spatial databases with noise. In *Proceedings of the second international conference on knowledge discovery and data mining* (Vol. 96, pp. 226–231).

Gallego, G., Delbruck, T., Orchard, G., Bartolozzi, C., Taba, B., Censi, A., … Scaramuzza, D. (2022). Event-based vision: A survey. *IEEE Transactions on Pattern Analysis and Machine Intelligence*, *44*(1), 154–180. doi: 10.1109/tpami.2020.3008413

Lomb, N. R. (1976). Least-squares frequency analysis of unequally spaced data. *Astrophysics and Space Science*, *39*(2), 447–462. doi: 10.1007/bf00648343

Mohri, K., Wohler, A., Weigand, B., & Schulz, C. (2015). Toluene laser-induced fluorescence (LIF) imaging of supersonic flow within a diverging duct with injectors in the supersonic region. In *29th international symposium on shock waves 1* (pp. 471–476). Springer International Publishing. doi: 10.1007/978-3-319-16835-7_74

Richter, J., Alexopoulos, C., & Weigand, B. (2022). Particle image velocimetry measurements in accelerated, transonic wake flows. *Flow, Turbulence and Combustion*, *109*(3), 667–696. doi: 10.1007/s10494-022-00339-5

Richter, J., Beuting, M., Schulz, C., & Weigand, B. (2019). Mixing processes in the transonic, accelerated wake of a central injector. *Physics of Fluids*, *31*(1), 016102. doi: 10.1063/1.5055749

Richter, J., Beuting, M., Steinhausen, C., Dreier, T., Schulz, C., & Weigand, B. (2017). Non-intrusive frequency measurements of bluff-body vortex shedding at high reynolds numbers. In *23rd international society of air-breathing engines conference.*

Scargle, J. D. (1982). Studies in astronomical time series analysis. II - Statistical aspects of spectral analysis of unevenly spaced data. *The Astrophysical Journal*, *263*, 835. doi: 10.1086/160554

Settles, G. S. (2001). *Schlieren and shadowgraph techniques*. Springer. doi: 10.1007/978-3-642-56640-0

Shiba, S., Hamann, F., Aoki, Y., & Gallego, G. (2023). Event-based background-oriented schlieren. *IEEE Transactions on Pattern Analysis and Machine Intelligence*, 1–16. doi: 10.1109/tpami.2023.3328188

Welch, P. (1967). The use of fast fourier transform for the estimation of power spectra: A method based on time averaging over short, modified periodograms. *IEEE Transactions on Audio and Electroacoustics*, *15*(2), 70–73. doi: 10.1109/tau.1967.1161901

Willert, C. E. (2023). Event-based imaging velocimetry using pulsed illumination. *Experiments in Fluids*, *64*(5). doi: 10.1007/s00348-023-03641-8

Willert, C. E., & Klinner, J. (2022). Event-based imaging velocimetry applied to a cylinder wake flow in air. *Proceedings of the International Symposium on the Application of Laser and Imaging Techniques to Fluid Mechanics*, *20*, 1–12. doi: 10.55037/lxlaser.20th.230

Williamson, C. H. K. (1996). Vortex dynamics in the cylinder wake. *Annual Review Fluid Dynamics*. doi: 10.1146/annurev.fl.28.010196.002401

Wohler, A., Weigand, B., Mohri, K., & Schulz, C. (2014). Mixing processes in a compressible accelerated nozzle flow with blunt-body wakes. *AIAA Journal*, *52*(3), 559–568. doi: 10.2514/1.j052493